N73 32615

NASA TECHNICAL MEMORANDUM

STUDIES OF DISHED ACCELERATOR GRIDS FOR 30-CM ION THRUSTERS

by Vincent K. Rawlin
Lewis Research Center
Cleveland, Ohio 44135

STUDIES OF DISHED ACCELERATOR GRIDS FOR 30-CM ION THRUSTERS

by Vincent K. Rawlin
National Aeronautics and Space Administration
Lewis Research Center
Cleveland, Ohio

Abstract

Eighteen geometrically different sets of dished accelerator grids were tested on five 30-cm thrusters. The geometric variation of the grids included the grid-to-grid spacing, the screen and accelerator hole diameters and thicknesses, the screen and accelerator open area fractions, ratio of dish depth to dish diameter, compensation, and aperture shape. In general, the data taken over a range of beam currents for each grid set included the minimum total accelerating voltage required to extract a given beam current and the minimum accelerator grid voltage required to prevent electron backstreaming.

Introduction

Recent studies of solar electric propulsion systems show a need for thruster arrays using 30-cm mercury bombardment ion thrusters[1,2]. Overall thruster efficiencies over 70 percent are desired at a maximum input power of approximately 2730 watts and a specific impulse of 3000 seconds. These requirements imply ion beam currents of about 2.0 amperes at net ion energies near 1100 electron-volts from a highly efficient discharge chamber. Reference 3 has shown that dished accelerator grids can easily extract a 2-ampere ion beam from a 30-cm thruster at net ion energies as low as 700 electron-volts. The major advantage which dished grids possess over flat grids with or without interelectrode supports, is that they can be reliably operated with small grid-to-grid spacings under repeated and long term thermal loading of thruster operation. Eighteen sets of dished grids (Table I) were tested to investigate the effects of grid geometry changes on ion beam extraction. The grid parameters varied were grid hole diameter, grid thickness, fraction open area, ratio of dish depth to dish diameter, compensation, and aperture shape. In addition, many grid sets were tested with various grid-to-grid spacings and several grid sets were tested on more than one of the five different 30-cm thrusters described in Table II.

The following performance parameters were evaluated at various beam currents: the minimum total voltage required to extract a given beam current, the minimum accelerator grid voltage required to prevent electron backstreaming, and the effects of the ratio of net-to-total accelerating voltage.

Apparatus and Procedure

Ion Accelerator Systems

The grid sets listed in Table I and used in this study were fabricated from arc-cast molybdenum as described in reference 3. The aperture sizes, shapes, and center-to-center spacings were varied as well as the dish depth. The grid-to-grid spacings was initially fixed by insulating spacers of synthetic mica for preliminary tests. For long duration tests the dished grids were mounted on molybdenum rings. The cold grid-to-grid spacings were measured by inserting "L" shaped "feeler" gauges, with known thicknesses, between the grids at many locations over the active area of the grid set. The average value of the spacings was used as the cold grid-to-grid spacing for Table III and it was estimated to be accurate to 0.03 mm. All the data presented were obtained with the grids dished away from the discharge chamber.

Thrusters

Five different 30-cm diameter thrusters were used to test the dished grids. They are described in Table II and references 4, 5, 6, and 7.

Facility and Power Supplies

All of the tests were conducted in the 3.0 m diameter bell jar of the 7.6 m diameter by 21.4 m long vacuum tank at the Lewis Research Center[8]. The bell jar pressure during thruster operation was 3×10^{-6} torr while the main tank pressure was 2×10^{-7} torr. Power to the thruster was supplied by d.c. and 60 Hertz a.c. power supplies.

Grid Performance Evaluation

The minimum total accelerating voltage, ΔV_M, required to extract a given beam current, J_B, was determined as described in reference 3 and is described briefly here for reference. All symbols are defined in the Appendix.

The minimum total accelerating voltage (the sum of the anode voltage plus the magnitude of the accelerator grid voltage) was determined by noting a rapid increase in the accelerator impingement current, J_A, with decreasing total voltage. This increase was caused by the inability of the grids to focus the ions through the accelerator holes. Data were obtained while maintaining constant J_B, discharge voltage, ratio of net-to-total accelerating voltage, and main propellant flow rate.

For purposes of grid comparison it is desirable to determine the ratio of J_B at ΔV_M to the theoretically predicted ion current. This ratio has been called the fraction or percentage of Child's law current in references 9 and 10 and is determined through the use of the space charge flow equation for parallel plates:

$$J_c = \frac{8}{9} \epsilon_o \sqrt{\frac{q}{2m}} \frac{A_s \Delta V_M^{\frac{3}{2}}}{\ell^2} \qquad (1)$$

where J_c is the calculated space charge limited ion current, ϵ_o is the permittivity of free space and q/m is the charge to mass ratio for ions which are assumed to be singly charged. A_s is the area of the ion source, assumed in references 9 and 10 to be the screen grid open area. ΔV_M is the

minimum total acceleration voltage determined by the above procedure. The ion accelerating distance, ℓ, is usually an estimated value which includes the cold grid-to-grid spacing plus some fraction of the screen and/or accelerator grid thicknesses. The value used for ℓ, in this report, will be defined at a later time.

The minimum accelerator voltage, V_{AM}, required to prevent electron backstreaming was measured for each grid set as a function of beam current, net accelerating voltage, and grid-to-grid spacing. At accelerator grid voltages slightly less than V_{AM} there was a rapid increase in the indicated J_B as electrons from the downstream plasma were able to backstream to the positive potential of the discharge chamber.

Results and Discussion

Minimum Total Accelerating Voltage

One method of evaluating the performance of ion extraction systems is to compare the current carrying capacity of each different set of grids. This can be accomplished by measuring the values of ΔV_M over a range of J_B for each grid geometry. This section will present data showing the effects of grid geometry and operating conditions on the current carrying capacities for the grids of Table I.

Effect of Thruster Type. Several sets of grids were tested on more than one of the thrusters listed in Table II. In no instance did the performance of any grid set depend significantly upon the thruster type. For example, grid set K was tested on all five thrusters with about a 3 percent variation in ΔV_M. It was therefore concluded that comparisons of different grids could be made on any of the five thrusters used in the program.

Effect of Discharge Power. The discharge power was increased by a factor of three while operating grid set M at a J_B of 2.0 amperes and a propellant utilization efficiency of 0.9 or more. The value of ΔV_M, as in reference 3, did not change with discharge power. In some tests, to obtain higher values of J_B, the total propellant flow rate was increased above normal because the discharge power was limited. This resulted in much lower propellant utilization and a more peaked plasma density which caused ion defocusing at higher than normal values of ΔV_M. All grid data was obtained at the highest value of propellant utilization obtainable unless stated otherwise. It was therefore concluded that the effective ion accelerating distance was unaffected and that different grids could be compared at different levels of discharge power as long as the propellant utilization efficiency was near the maximum possible value.

Effect of the Ratio of Net-to-Total Accelerating Voltage, R. The ΔV_M was measured for several grid sets over a range of J_B as the ratio of the net-to-total accelerating voltage, R, was varied. No noticeable change occurred in ΔV_M when R was decreased from the maximum value (where electron back-streaming occurred) to about 0.4. This was similar to the results of reference 3. At values of R less than 0.4, the accelerator impingement current increased because of defocused

ions, which made it difficult to determine ΔV_M. It was therefore concluded that grid sets could be compared at different values of R when R was greater than 0.4. The data of Table III were obtained at values of R between 0.57 and 0.70.

Effect of Beam Current. Figure 1 is a log-log plot of the values of ΔV_M at various values of J_B for grid set D taken from Table III. The different curves are for different grid-to-grid spacings. Estimated ion accelerating distances, which will be defined later, are shown in Fig. 1. Figure 1 is typical, in several respects, to the results with the other grid geometries. For a fixed ℓ, the functional relationship of ΔV_M to J_B was constant over a large range of J_B, with the exception of tests 6 and 7 where, as indicated previously, abnormally high values of ΔV_M at increased values of J_B probably resulted from decreased propellant utilization efficiency. In Fig. 1, J_B increased at a power of ΔV_M greater than the 3/2 power predicted by Eq. (1), for each of the five estimated ion acceleration distances which were varied from 0.98 to 1.41 mm. This was also found in reference 3 and was true for all of the dished grid sets presented herein.

The exact reasons for the deviations from the functional dependence predicted by Eq. (1) are not known. Several phenomena could explain this behavior. They include the variation of effective accelerating distance with J_B (and ΔV_M), variation of beam profiles with J_B, doubly charged ions, and ions with initial velocities. Also, the multiaperture grids tested, are significantly different than the planar diodes assumed in the derivation of Eq. (1). These different effects will be discussed briefly.

1. Variation of effective ion accelerating distance with J_B. The grid-to-grid spacing could change with discharge power variations as J_B is varied. Such power variations would be expected to vary the absolute temperatures and possibly the thermal profiles of both grids. As indicated earlier however, the effects of discharge power variation were insignificant. The grid-to-grid spacing could change with applied voltage as a result of electrostatic forces. Preliminary tests, in atmosphere, indicate that over the range of total accelerating voltages presented herein, there was no observable change in grid spacing with applied voltage. Attempts to measure changes in grid spacing during operation have been unsuccessful. The effective ion accelerating distance could vary if the upstream or downstream plasma boundaries moved as the thruster operating conditions were changed. This has been indicated by Lathem in reference 11.

2. Variation of beam profile with J_B. Beam profile changes could lead to ion defocusing at a different radial position on the grid. Since the grid-to-grid spacing is not uniform across the grid during operation, ion defocusing at a different radial location probably would result in a different ℓ. Preliminary measurements of beam profiles obtained from a planar probe located 2 cm downstream of the grids have indicated that the shape of the beam profile was not a function of J_B but was slightly dependent on the total accelerating voltage.

3. Doubly charged ions. The mercury plasma contains doubly-charged as well as singly-charged ions[12, 13]. Reference 13 has shown that the integrated double ion content of the ion beam increases with J_B. The exact extent of the effect of doubly-charged ions is not known but it would contribute to the increased sensitivity of J_B to ΔV_M observed in Fig. 1.

4. Initial ion velocity. The initial velocity acquired by the ions as they approach the accelerating region, in effect, allows a reduction of the total accelerating voltage. But the variations of this velocity with variations in J_B are only on the order of a few volts and should not significantly affect the values of ΔV_M[14].

5. Multi-aperture grids. Equation (1) was derived for a vacuum diode consisting of two parallel plates separated by a uniform spacing. In reality, the accelerator grid set consists of two perforated plates separated by a non-uniform spacing during operation. The effect of the holes, on the variation of grid performance with J_B is not known.

Effect of Grid Geometry. This section will present the effects on ΔV_M of changes in the geometry of the grid set. The results of some of these changes were strongly interrelated. Attempts will be made to separate the results for clarity.

1. Estimated ion accelerating distance, ℓ. From Fig. 1 it can be seen that the performance of the dished grids was a strong function of ℓ and that some estimate of the ion accelerating distance was required to compare the experimental results. Reference 3 used the sum of the screen grid thickness and the cold grid-to-grid spacing minus the change in spacing due to thermal loading as the estimated ion accelerating distance. There, the change in effective spacing was estimated to be 0.26 mm. The results of this program, where the accelerator grid thickness was varied, indicated that the accelerator grid thickness also was important in the determination of the level of extracted ion current. As will be discussed later, three-fourths of the accelerator grid thickness was added to the ℓ of reference 3. Thus, the ℓ used herein is defined as the sum of the screen grid thickness, the cold grid-to-grid spacing, and three-fourths of the accelerator grid thickness minus 0.26 mm for grids with a ratio of dish depth to dish diameter of 0.075. Results with grids with a ratio of dish depth to dish diameter of 0.038 indicated the change in spacing, when operated, to be 0.74 mm and this value, rather than 0.26 mm, was used for those grids with the shallower dish depth.

It should be noted that the selection of this distance was somewhat arbitrary and was chosen as a convenience for the purpose of comparing the different grid types with each other as well as with Eq. (1).

Values of ΔV_M are plotted in Fig. 2 as a function of ℓ for all of the grid sets of Table III operated at a beam current of 2.0 amperes. Note that most of the data lie in a band in which ΔV_M increases with ℓ, but in general, slower than the 4/3 power predicted by Eq. (1).

When the values of ΔV_M for other values of J_B were plotted as a function of ℓ, the trends

were the same as those shown in Fig. 2. For this reason, subsequent discussion of the effects of grid geometry variations on grid performance will be made by comparing values of ΔV_M obtained for operation at J_B of 2.0 amperes only. For completeness, the data at all beam currents is presented in Table III.

Figure 2 can be used to estimate the cold grid-to-grid spacing required for a large range of dished grid geometries operated at a value of J_B of 2.0 amperes. All that is needed is a knowledge of the ΔV_M required and the thickness of the screen and accelerator grid.

2. Effect of accelerator grid thickness, t_A. Figures 3(a) and (b) compare the performance of grid set D with E (screen grid open area fraction, $F_{OS} = 0.51$) and grid set M with N ($F_{OS} = 0.67$) where the only difference, in each case was t_A. In both instances, the data followed similar trends when the estimated ion accelerating distance included three-fourths of the accelerator grid thickness. When the fraction of t_A was omitted from the estimated ℓ, as in reference 3, the values of ΔV_M were greater for the grids with the larger t_A. This probably occurred because the maximum beamlet diameter in the accelerator hole increased when t_A was increased[15].

3. Effect of screen grid thickness, t_S. Figure 3(a) compares the performance of grid sets D and F, which were identical except that t_S for grid set F was twice that of D. When the larger value of t_S was entirely accounted for in ℓ, the performance difference was negligible. Comparison of tests 8 and 10 of Table III shows that even though the cold spacings were 0.99 and 0.66 mm for grid D and F, respectively, the estimated values of ℓ were 1.12 and 1.17 and that the values of ΔV_M over a range of J_B were nearly identical.

4. Effects of screen and accelerator grid hole diameters, d_S, d_A. Figure 4 compares the performance of several grid sets in which only the grid hole diameters were varied. Figure 4(a) shows the variation of grid performance with hole diameter for grid sets B, C, and D where F_{OS} and F_{OA} were 0.51. There are only single data points for grid sets B and C because the discharge chamber performance with those grids was relatively poor. For grid set D (d_S and d_A = 1.91 mm), Fig. 4(a) shows that there was an increasing sensitivity of ΔV_M to ℓ as ℓ increased. Also the grids with smaller holes had larger values of ΔV_M than grid set D. It is possible that the non-linear effect for grid set D and the increased values of ΔV_M for grid sets B and C are due to grid open area variations. As suggested in reference 7, to explain the sensitivity of the discharge chamber performance to ℓ for grids with F_{OS} of 0.51, the effective screen grid hole diameter (plasma surface available for ion extraction) may have been greater than the physical d_S. It also may have increased with decreasing ℓ and increasing d_S.

Figures 4(b) and (c) also show the effect of grid hole diameter on ΔV_M, but for grids with F_{OS} of 0.67 and F_{OA} of 0.67 and 0.43, respectively. They are both linear with ℓ and show little or no sensitivity of ΔV_M to d_S. The probable explanation is that the effective screen grid hole diameter had reached a maximum value for high physical open area grids and was insensitive to

variations in d_S or ℓ. The same explanation was offered in reference 7 when there were negligible variations in the discharge chamber performance for grids with F_{OS} of 0.67. Comparison of Fig. 4(b) to 4(c) shows that the slope of Fig. 4(b) (grids with equal hole diameters) was steeper than Fig. 4(c) ($d_A = 0.8 \, d_S$). This effect cannot be explained at this time.

6. **Effect of screen and accelerator grid open area fraction, F_{OS}, F_{OA}.** Figure 5 compares the performance of several grid sets each having equal values of F_{OS} and F_{OA} which ranged from 0.43 to 0.77. With the exception of grid set A ($F_{OS} = 0.43$), the performance of the grids was insensitive to variations in F_{OS}. The probable explanation, as presented earlier, is that the effective F_{OS} was larger than the physical F_{OS} and near the maximum of unity for most grids, and therefore insensitive to changes in the physical F_{OS}. The higher value of ΔV_M for grid set A can be attributed to the possibility that the effective F_{OS} was closer in value to the physical F_{OS}, as discussed earlier.

7. **Effect of hole pattern compensation.** Figure 6 compares the performance of several grid sets with different amounts of grid hold pattern compensation[16]. Compensation (expressed as a percent strain) adjusts the grid hole center-to-center spacing in a manner which reduces the thrust loss due to beam divergence. For grids with two different geometries, the values of ΔV_M were unaffected by grid hole compensation up to 0.66 percent for grids with F_{OA} of 0.51 and 0.35 percent for grids with F_{OA} of 0.43.

8. **Effect of ratio of dish depth to dish diameter, h/D.** Reference 3 predicted twice the change in spacing due to thermal loading for dished grids with half the h/D. Comparison of tests 32 and 35 show that nearly the same performance was obtained, for grid sets R and S, even though the cold grid spacing differed by more than a factor of two. By assuming that grids with the same performance have the same effective ℓ, the change in spacing due to thermal loading was estimated to be 0.74 mm. When this value was used in ℓ, for all of the tests of grid set S, the performance was equivalent to that of grid set R over a wide range of ℓ as shown in Fig. 7.

Ratio of Experimental J_B to Calculated J_C.

The space charge limited current, J_C, was calculated, from Eq. (1), for all of the tests of Table III. The value of A_S used was taken to be 6.6×10^4 sq. mm, the total area of the perforated region of the screen grid without concern for the physical blockage of the webs between the holes. This assumption was made because it was shown earlier that the performance of all but one of the grid sets was insensitive to the physical open area fraction. The ℓ used in the calculation was as defined in the section entitled "Estimated ion accelerating distance." The charge to mass ratio for singly charged ions was used. Using the experimental values of ΔV_M, values of J_C were obtained. The ratios of the corresponding experimental J_B to the calculated value of J_C are listed in Table III. Table III shows that in most cases the ratio increased with J_B for a fixed ℓ.

Figure 8 shows that in general, the ratio of J_B to J_C increased with ℓ when the grids of Table I were operated at a J_B of 2.0 ampere. This effect possibly can be explained by the grid aperture effect which was discussed in reference 9. Theoretically the ratio of J_B to J_C should increase with the ratio of ℓ to d_S and with R. Since the values of ΔV_M were not sensitive to most variations in d_S or variations of R when R was greater than 0.4, the ratio of J_B to J_C were plotted as a function of ℓ only.

Minimum Accelerator Grid Voltage

To maximize the accelerator grid lifetime, it is desirable to minimize the accelerator grid voltage in order to reduce the sputtering erosion of incident ions. Reference 16 has also shown that to minimize the thrust loss due to beam divergence it is desirable to maximize the ratio of net-to-total accelerating voltage, R. The maximum value of R is limited to that value which prevents electron backstreaming, therefore those parameters which affect R were studied.

Effect of Beam Current, J_B. Figure 9 shows the variation of the minimum accelerator grid voltage, V_{AM}, with J_B for most of the grids of Table I. For a given grid set V_{AM} increased gradually with J_B, increasing only about 80 volts for the most sensitive grid set, as J_B was increased from 1.0 to 2.0 amperes.

Effect of Estimated Ion Accelerating Distance, ℓ. Values of V_{AM} were obtained for several grid sets tested over a range of ℓ. V_{AM} was not a strong function of ℓ but did decrease slightly as ℓ was increased.

Effect of Net Ion Accelerating Voltage, V_I. Figure 10 presents the variation of V_{AM} with V_I for three values of J_B for test 20 using grid set M. In all cases, V_{AM} increased about 20 volts for every 100 volt increase in V_I. Therefore, if a use of electric propulsion requires an increasing V_I, an increase in V_A may also be required to avoid electron backstreaming.

Effect of Accelerator Grid Thickness, t_A. Figure 11 shows the variation of V_{AM} with J_B for two pairs of grid sets in which only t_A was varied. When t_A was doubled for grid set E, V_{AM} decreased approximately 100 volts at a J_B of 2.0 amp. The t_A for grid set M was increased by 50 percent for grid set N which resulted in a decrease of V_{AM} of about 50 volts. In both cases the increase of t_A provided more of a shield of the positive potentials from the neutralizing electrons in the ion beam.

Effect of Accelerator Grid Hole Diameter, d_A. To separate the effect of d_A from the effects of J_B and t_A variations, values of V_{AM} obtained at J_B of 2.0 amperes for only those grid sets with t_A equal to 0.38, were plotted in Fig. 12 as a function of d_A. As d_A was increased from 1.02 to 2.41 mm V_{AM} also increased from about 140 to 450 volts. The accelerator grid hole diameter had the strongest effect on V_{AM} of any parameter studied and was the chief factor in the determination of the maximum value of the ratio of the net-to-total accelerating voltage.

4

Grid Lifetime

Table I lists the total test time in hours that each grid set was operated. The total accumulated test time for the sixteen grid sets used in this study was 4584 hours. Grid sets D and H each had more than 1550 hours with most of the time occurring at J_B of 2.0 to 2.5 amperes. Grid performance has been extremely repeatable during extended tests and from test-to-test.

None of the grids tested show wear on the accelerator grid due to neutralizer ions. This resulted from repositioning the neutralizer away from the accelerator grid as suggested by Bechtel in reference 17 and the accelerator grid voltage was 500 volts or less. Typical values of impingement current were 0.2 to 0.3 percent of the beam current. For the grid sets with 1550 accumulated hours the pattern of charge-exchange erosion was visible on the downstream side of the accelerator and was approximately measured to be 0.01 mm deep at the most.

Conclusions

The minimum total accelerating voltage was measured for eighteen different grid geometries operated over a range of beam currents and grid spacings. The minimum total accelerating voltage was found to be insensitive to thruster type, discharge power variations, and the ratio of the net-to-total accelerating voltage when R was greater than 0.4. When compared at a constant value of beam current, the minimum total accelerating voltages, for the dished grids tested in this program having an open area fraction of 0.51 or greater and a screen hole diameter of 1.91 or greater, were primarily a function of only the estimated ion accelerating distance. The ion accelerating distance was estimated to be the sum of the screen grid thickness, the cold grid-to-grid spacing, and three-fourths of the accelerator grid thickness minus the change in the grid-to-grid spacing due to the thermal loading of thruster operation. This insensitivity of the minimum total accelerating voltage to grid geometry changes, other than the estimated ion accelerating distance, led to the conclusion that the effective screen grid open area fraction was constant and nearly unity and therefore unaffected by screen grid hole diameter changes.

Values of space-charge limited ion current were calculated using the experimental values of the minimum total accelerating voltage and the estimated ion accelerating distances. The ratios of experimental beam current to the calculated space charge limited ion current were found to increase with estimated ion accelerating distance at a fixed beam current.

The minimum accelerator grid voltage, required to prevent electron backstreaming to the discharge chamber, increased slightly with increasing ion beam current, decreasing estimated ion accelerating distance, increasing net accelerating voltage, and decreasing accelerator grid thickness. The minimum accelerator grid voltage was found to be a strong function of the accelerator grid hole diameter.

Two sets of dished grids, used in this program, have each accumulated more than 1550 hours

of repeatable thruster operation. None of the grids tested had wear from neutralizer ions or charge-exchange ions greater than 0.01 mm in depth.

Appendix

Symbols

A_S — Area of the ion source, mm^2.

d_A — Accelerator grid hole diameter, mm.

d_S — Screen grid hole diameter, mm.

F_{OA} — Accelerator grid open area fraction.

F_{OS} — Screen grid open area fraction.

h/D — Ratio of dish depth to dish diameter.

J_A — Accelerator grid impingement current, ma.

J_B — Ion beam current, amp.

J_C — Space charge limited current, amp.

ℓ — Estimated ion accelerating distance, mm.

q/m — Charge-to-mass ratio for singly-charged mercury ions, 0.4811×10^6 coulomb/kg.

R — Ratio of net-to-total accelerating voltage.

t_A — Accelerator grid thickness, mm.

t_S — Screen grid thickness, mm.

V_A — Accelerator grid voltage, volts.

V_I — Net ion accelerating voltage, volts.

V_{AM} — Minimum accelerator grid voltage, volts.

ΔV_M — Minimum total accelerating voltage.

ϵ_o — Permittivity of free space, 8.85×10^{-12} $coulomb^2/nt \cdot m$.

References

1. Gardner, J. A., "Solar Electric Propulsion System Integration Technology (SEPSIT). Vol III: Supporting Analysis," TM 33-583, Vol. III, NASA CR-130703, Nov. 1972, Jet Propulsion Lab., Pasadena, Calif.

2. Anon., "Study of a Common Solar-Electric-Propulsion Upper Stage for High-Energy Unmanned Missions. Vol. 2: Technical," Rep. TRW-16552-6007-RO-00-Vol. 2, NASA CR-114350, July 1971, TRW Systems Group, Redondo Beach, Calif.

3. Rawlin, V. K., Banks, B. A., and Byers, D. C., "Dished Accelerator Grids on a 30-cm Ion Thruster," Journal of Spacecraft and Rockets, Vol. 10, No. 1, Jan. 1973, pp. 29-35.

4. Bechtel, R. T., "Performance and Control of a 30-cm-Diam, Low-Impulse Kaufman Thruster," Journal of Spacecraft and Rockets, Vol. 7, No. 1, Jan. 1970, pp. 21-25.

5. King, H. J., and Poeschel, R. L., "Low Specific Impulse Ion Engine," NASA CR-72677, Feb. 1970, Hughes Research Labs., Malibu, Calif.

6. Anon., "Low Voltage 30-cm Ion Thruster," NASA CR-120919, Feb. 1972, Hughes Research Labs., Malibu, Calif.

7. Rawlin, V. K., "Performance of 30-cm Ion Thrusters with Dished Accelerator Grids," paper to be presented at the AIAA 10th Electric Propulsion Conference, Oct. 31-Nov. 2, 1973.

8. Finke, R. C., Holmes, A. D., and Keller, T. A., "Space Environment Facility for Electric Propulsion Systems Research," TN D-2774, 1965, NASA, Cleveland, Ohio.

9. Kerslake, W. R., "Accelerator Grid Tests on an Electric-Bombardment Ion Rocket," TN D-1168, 1962, NASA, Cleveland, Ohio.

10. Kerslake, W. R., and Pawlik, E. V., "Additional Studies of Screen and Accelerator Grids for Electric-Bombardment Ion Thrusters," TN D-1411, 1963, NASA, Cleveland, Ohio

11. Lathem, W. C., "Analytic Performance of Two-Grid Accelerator Designs for Kaufman Thrusters," TN D-6275, 1971, NASA, Cleveland, Ohio.

12. Pawlik, E. V., Goldstein, R., Fitzgerald, D. J., and Adams, R. W., "Ion Thruster Performance Calibration," Paper 72-475, Apr. 1972, AIAA, New York, N.Y.

13. Vahrenkamp, R., "Measurement of the Double Ion Content of the 30-cm Mercury Bombardment Thrusters," AIAA paper to be presented at the 10th Electric Propulsion Conf., Oct. 31-Nov. 2, 1973.

14. Howes, W. L., "Effect of Initial Velocity on One-Dimensional, Ripolar, Space-Charge Currents," Journal of Applied Physics, Vol. 36, No. 6, June, 1965, pp. 2039-2045.

15. Lathem, W. C., "Ion Accelerator Designs for Kaufman Thrusters," Paper 69-261, Mar. 1969, AIAA, New York, N.Y.

16. Danilowicz, R. L., Rawlin, V. K., Banks, B. A., and Wintucky, E. G., "Measurement of Beam Divergence of 30-cm Diameter Dished Grids," AIAA paper to be presented at the 10th Electric Propulsion Conference, Oct. 31-Nov. 2, 1973.

17. Bechtel, R. T., "Performance of a Neutralizer for Electron Bombardment Thruster," Paper 72-207, Jan. 1972, AIAA, New York, N.Y.

Table I - Dished Grid Geometry

Grid set	Hole diameter, mm		Grid thickness, mm		Open area fraction		Compensation, ε%	Aperture shape	Ration of dish depth to dish diameter	Total test time, hr
	Screen	Accelerator	Screen	Accelerator	Screen	Accelerator				
A	1.52	1.52	0.51	0.51	0.43	0.43	0	Circular	0.075	84
B	1.02	1.02	0.38	0.38	0.51	0.51	0	Circular	0.075	7
C	1.27	1.27	.38	.38	↓	↓		↓	↓	52
D	1.91	1.91	.38	.38						1552
E	↓	↓	.38	.76						5
F			.76	.38						5
G			.38	.38			0.22			6
H			.38	.38			.44			33
J	↓	↓	.38	.38	↓	↓	.66	↓	↓	13
K	1.91	1.91	0.38	0.38	0.67	0.67	0	Circular	0.075	1580
L	2.41	2.41	.38	.38	.67	.67	0	Circular	.075	205
M	1.91	1.52	0.38	0.51	0.67	0.43	0	Circular	0.075	332
N	1.91	1.52	↓	.76	↓	↓	0	↓	↓	382
O	1.91	1.52		.76			0.35			73
P	2.16	1.73		.76			0			10
Q	2.41	1.93	↓	.76	↓	↓	0	↓	↓	135
R	2.08	2.08	0.38	0.38	0.77	0.77	0	Hexagonal	0.075	110
S	2.08	2.08	.38	.38	.77	.77	0.097	Hexagonal	.038	23

Table II - 30 cm Thruster Geometry

Thruster	Basic thruster design	Thruster description	Major differences from basic design
A	LeRC	Ref. 4	None
B	HRL300	Ref. 5	None
C	HRL400	Ref. 6	Active magnetic baffle
D	HRL300	Ref. 1	Active magnetic baffle, axial and radial electromagnets
E	HRL400	Ref. 1	Active magnetic baffle, shorter cathode pole piece, stronger magnetic field

Table III - Performance of Grids of Table I

Test	Thruster	Grid set	Cold grid spacing, mm	Estimated ion accelerating distance, ℓ, mm	Beam current, J_B, A	Minimum total accelerating voltage, ΔV_M, v	Ratio of experimental J_B to calculated J_C, percent	Maximum R
1	B	A	0.76	1.40	0.7 1.0 1.5 2.0	920 1120 1370 1680	19.2 20.6 22.7 22.6	0.90
2	C	B	0.56	0.98	1.0 1.5 2.0	900 960 1080	14.0 19.2 24.3	0.90
3	B	C	0.86	1.28	1.0 1.5 2.0	1300 1530 1690	13.8 16.2 18.5	0.90
4	B	D	0.56	0.98	1.0 1.5 2.0 2.5	680 810 940 1040	21.3 24.5 26.2 28.2	0.75
5	B	D	0.66	1.08	0.7 1.0 1.5 2.0 2.5	630 720 870 1000 1090	23.0 27.0 30.5 32.9 36.1	0.75
6	B	D	0.81	1.23	0.7 1.5 2.0 2.5 2.9	740 960 1140 1350 1650	20.7 30.2 31.0 30.1 25.8	0.76
7	B	D	0.86	1.28	0.7 1.5 2.0 2.5 3.0	740 1000 1140 1260 1420	22.4 30.4 33.5 36.0 36.2	0.76
8	A	D	0.99	1.41	1.0 1.5 2.0	1030 1210 1380	25.5 27.8 30.5	0.78

Table III - Performance of Grids of Table I (cont.)

Test	Thruster	Grid set	Cold grid spacing mm	Estimated ion accelerating distance, ℓ, mm	Beam current, J_B, A	Minimum total accelerating voltage, ΔV_M, v	Ratio of experimental J_B to calculated J_C, percent	Maximum R
9	E	E	0.66	1.36	0.5 1.0 2.0	790 950 1270	16.4 25.9 32.2	0.85
10	E	F	0.66	1.46	0.5 1.0 1.5 2.0	790 1040 1220 1430	13.3 25.9 28.8 31.0	0.80
11	C	G	0.51	0.93	2.0	890	25.6	0.75
12	E	H	0.81	1.23	1.0 1.5 2.0	880 1090 1220	22.8 25.9 28.0	0.75
13	C	J	0.86	1.28	1.0 1.5 2.0	840 1040 1250	26.4 28.8 29.2	0.78
14	B	K	0.66	1.08	1.0 1.5 2.0	790 900 1010	20.7 25.5 28.9	0.74
15	A	K	0.73	1.15	1.0 1.5 2.0	900 1010 1130	19.2 24.3 27.3	0.76
16	B	L	0.58	1.00	1.0 1.5 2.0 2.5 3.0	610 730 860 960 1120	26.0 30.7 31.3 33.1 31.4	0.70
17	B	L	0.76	1.18	1.5 2.0 2.5 3.0	940 1130 1260 1380	28.7 28.9 30.8 32.3	0.71
18	B	L	1.02	1.43	1.0 1.5 2.0 2.5 3.0 3.5 4.0	1020 1250 1470 1660 1820 2400 2830	24.8 27.4 28.6 29.8 31.1 24.0 21.4	0.78
19	E	M	0.46	0.97	1.0	790	16.7	0.82
20	E	M	0.68	1.19	1.0 1.5 2.0	940 1040 1090	19.4 24.9 30.9	0.84
21	E	M	0.73	1.24	0.5 1.0 1.5 2.0 2.5	810 940 1080 1120 1240	13.2 21.0 25.5 32.2 34.7	0.85
22	E	M	0.92	1.42	2.0	1280	34.6	0.86
23	E	N	0.51	1.21	1.35 2.0	960 1110	26.2 31.0	0.80

Table III - Performance of Grids of Table I (conc.)

| Test	Thruster	Grid set	Cold grid spacing mm	Estimated ion accelerating distance, ℓ, mm	Beam current, J_B, A	Minimum total accelerating voltage, ΔV_M, v	Ratio of experimental J_B to calculated J_C, percent	Maximum R
24	E	N	0.63	1.33	1.0 1.5 2.0	940 1060 1200	24.2 31.6 33.4	0.84
25	E	N	0.97	1.66	0.8 1.0 2.0	1060 1160 1460	25.1 27.7 38.8	0.86
26	D	O	0.92	1.61	2.0	1350	41.0	0.89
27	C	P	1.02	1.71	1.0 1.5 2.0	1130 1270 1360	30.2 39.1 45.8	0.82
28	B	Q	0.76	1.46	1.5 2.0	1130 1260	30.3 34.4	0.80
29	A	Q	0.84	1.54	1.5 2.0	1200 1360	29.5 32.6	0.82
30	C	Q	0.94	1.64	1.0 1.5 2.0	1180 1370 1500	23.0 27.4 32.2	0.83
31	C	Q	1.25	1.94	1.0 1.5 2.0	1410 1560 1620	28.0 36.2 45.5	0.84
32	B	R	0.43	0.85	1.5 2.0 2.5 3.0 4.0 5.0	790 900 960 1050 1300 1800	19.1 20.9 23.4 24.9 24.0 19.3	0.64
33	C	R	1.14	1.56	1.0 2.0	980 1340	31.2 39.1	0.73
34	B	R	1.40	1.82	1.0 1.5 2.0 2.5	1020 1240 1480 1620	40.0 44.8 45.8 50.0	0.74
35	C	S	0.91	0.85	1.0 1.5 2.0	630 770 880	17.8 19.8 21.7	0.73
36	C	S	1.17	1.10	1.0 1.5 2.0	830 920 1010	19.8 25.5 29.5	0.73
37	C	S	1.98	1.92	1.0 1.5 2.0	1400 1450 1510	27.7 39.3 49.3	0.77
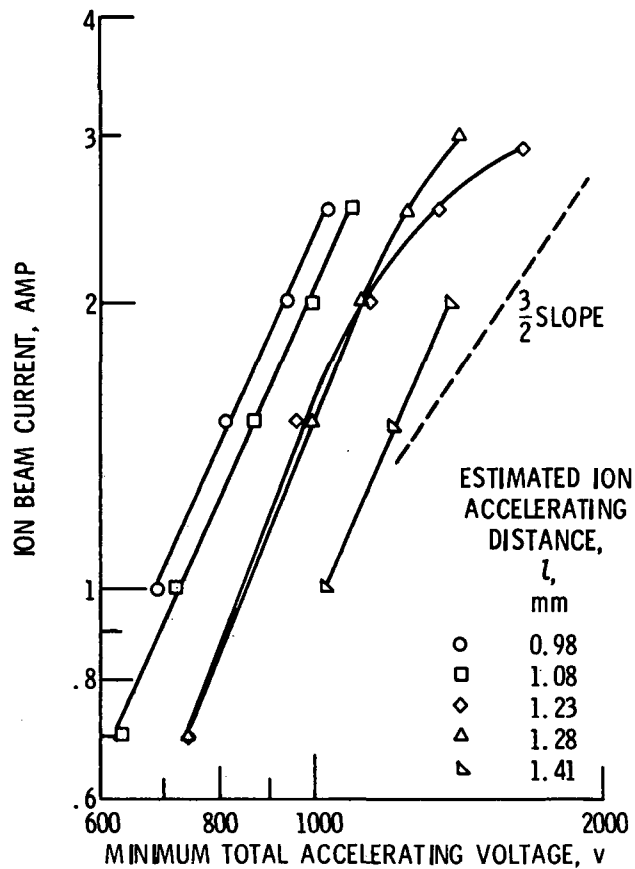
Figure 1. - Ion beam current as a function of minimum total accelerating voltage for grid set D.
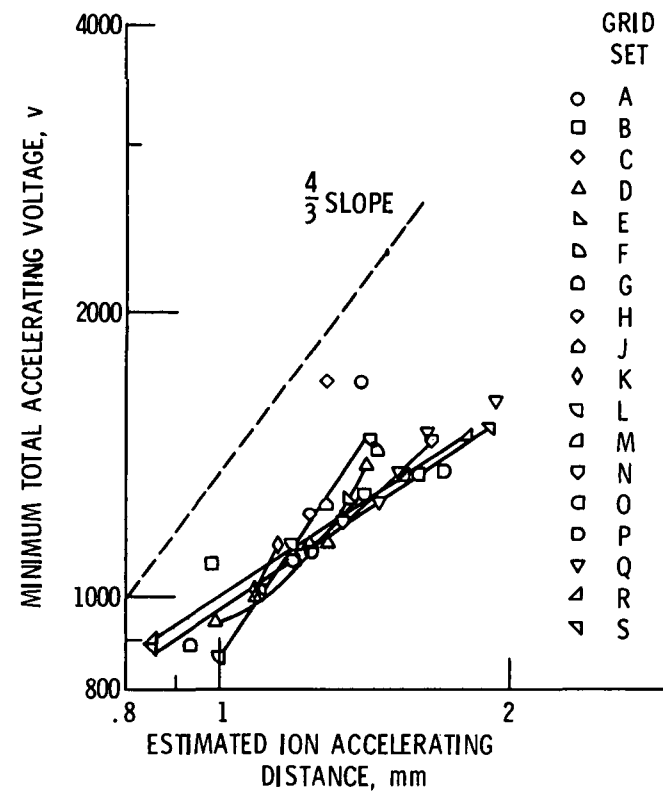

Figure 2. - Minimum total accelerating voltage as a function of estimated ion accelerating distance for grid sets of table III operated at 2.0 amperes beam current.
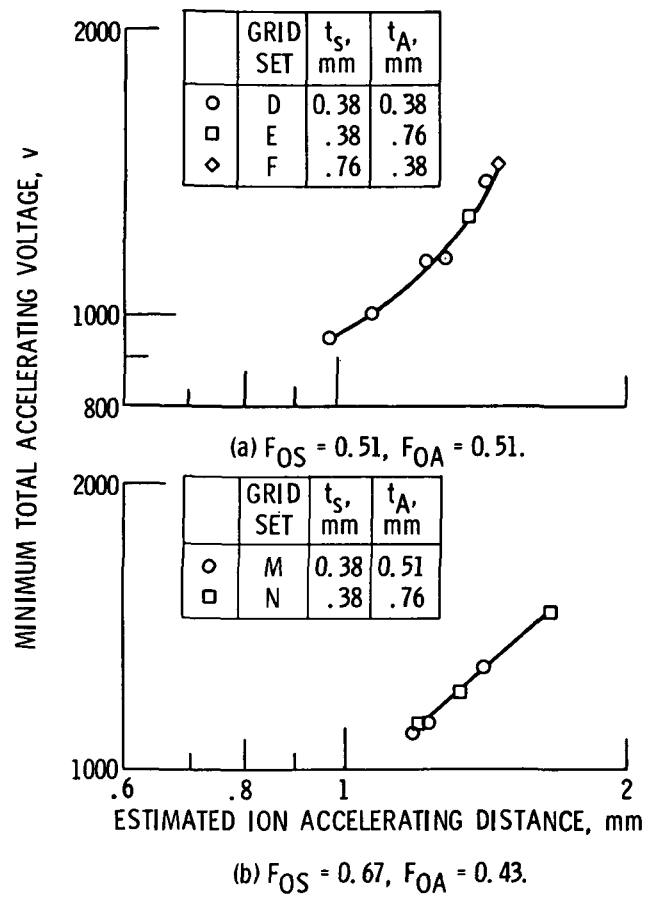
Figure 3. – Grid performance variation with
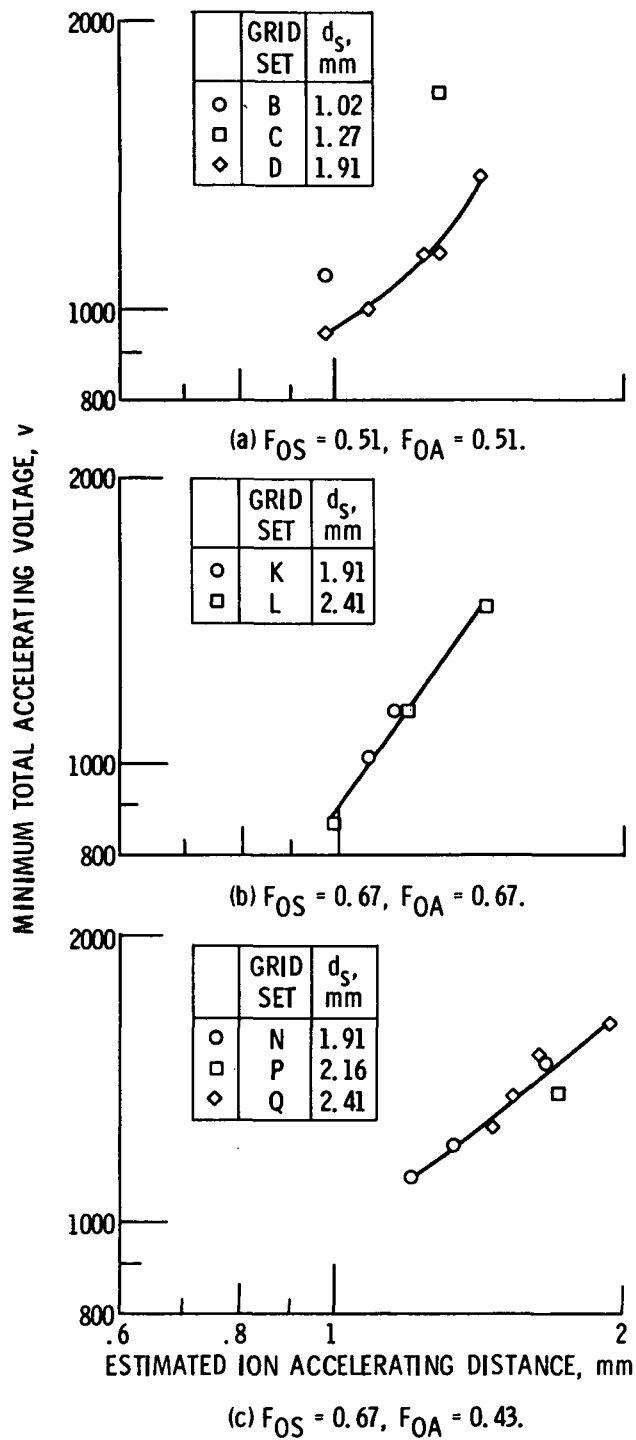screen and acceleration grid thickness.

MINIMUM TOTAL ACCELERATING VOLTAGE, V

2000

	GRID SET	d_s, mm
○	B	1.02
□	C	1.27
◇	D	1.91

1000

800

(a) $F_{OS} = 0.51$, $F_{OA} = 0.51$.

2000

	GRID SET	d_s, mm
○	K	1.91
□	L	2.41

1000

800

(b) $F_{OS} = 0.67$, $F_{OA} = 0.67$.

2000

	GRID SET	d_s, mm
○	N	1.91
□	P	2.16
◇	Q	2.41

1000

800

.6 .8 1 2

ESTIMATED ION ACCELERATING DISTANCE, mm

(c) $F_{OS} = 0.67$, $F_{OA} = 0.43$.

Figure 4. – Grid performance variation with screen and accelerator grid hole diameters.

	GRID SET	F_{OS}	F_{OA}	d_{s}, mm
○	A	0.43	0.43	1.52
□	D	.51	.51	1.91
◇	K	.67	.67	1.91
△	R	.77	.77	2.08
◭	S	.77	.77	2.08

ESTIMATED ION ACCELERATING DISTANCE, mm
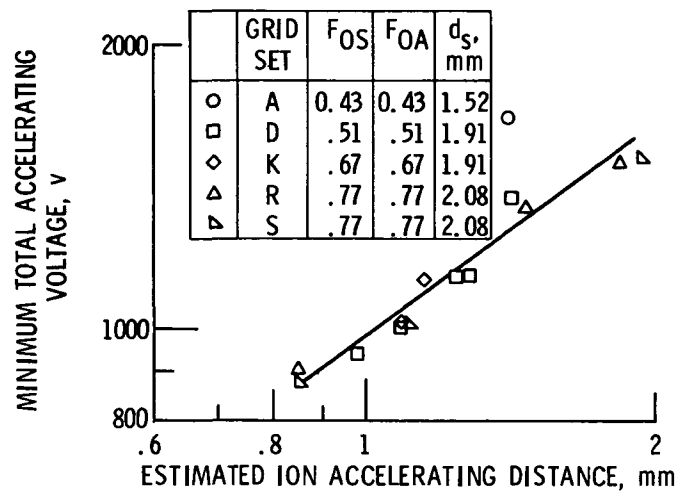
Figure 5. – Grid performance variation with screen and accelerator grid open area fractions.

	GRID SET	% STRAIN	F_{OA}
○	D	0	0.51
□	G	.22	.51
◇	H	.44	.51
△	J	.66	.51
◣	N	0	.43
◤	O	.35	.43

ESTIMATED ION ACCELERATING DISTANCE, mm
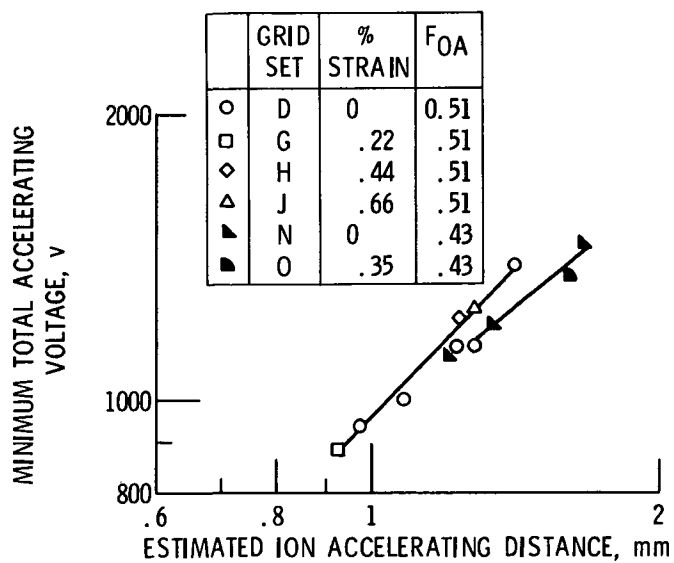
Figure 6. – Grid performance variation with grid hole pattern compensation.

MINIMUM TOTAL ACCELERATING VOLTAGE, V

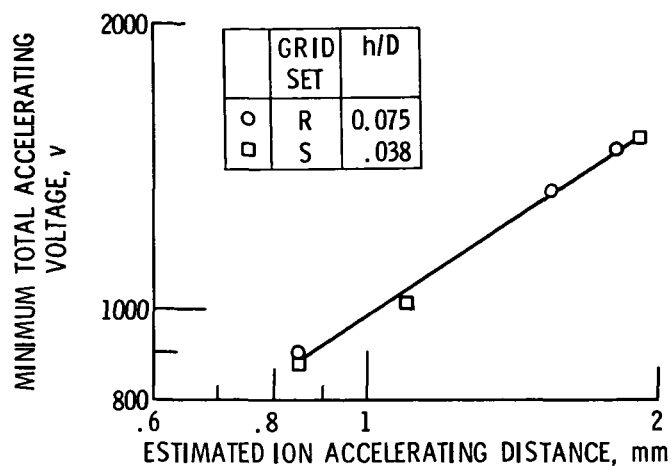|	GRID SET	h/D
○	R	0.075
□	S	.038

ESTIMATED ION ACCELERATING DISTANCE, mm

Figure 7. - Grid performance variation with ratio of dish depth to dish diameter.

RATIO OF EXPERIMENTAL BEAM CURRENT TO CALCULATED SPACE CHARGE LIMITED CURRENT, PERCENT

GRID SET					
○	A	◖	G	▽	N
□	B	◇	H	◁	O
◇	C	◬	J	▢	P
△	D	◈	K	▽	Q
▷	E	◁	L	◮	R
◭	F	◰	M	◀	S

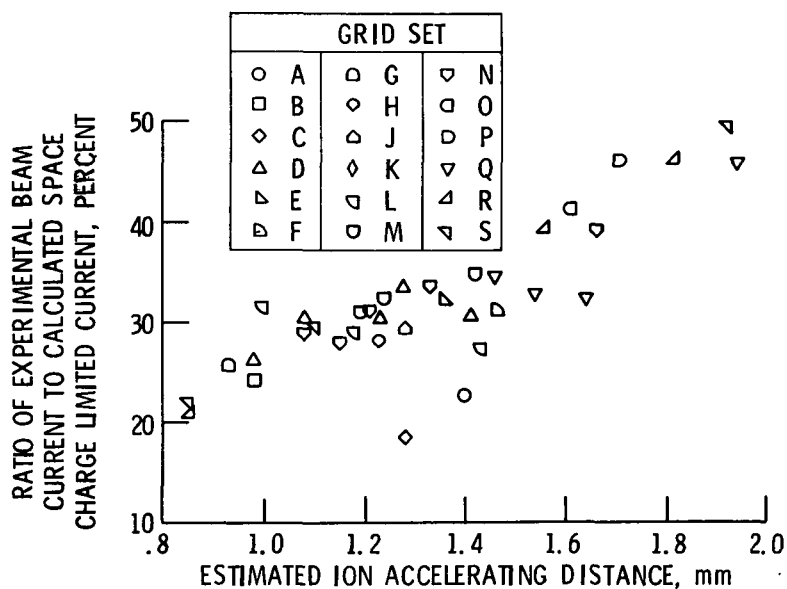ESTIMATED ION ACCELERATING DISTANCE, mm

Figure 8. - Ratio of experimental beam current to cal-
culated space charge limited current as a function
of estimated ion accelerating distance for an experi-
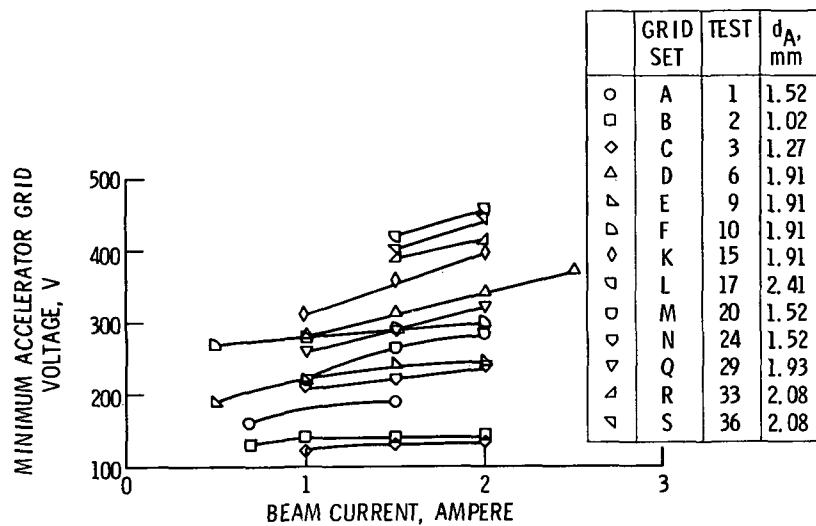mental beam current of 2.0 amperes.

	GRID SET	TEST	d_A, mm
○	A	1	1.52
□	B	2	1.02
◇	C	3	1.27
△	D	6	1.91
◮	E	9	1.91
◹	F	10	1.91
◈	K	15	1.91
◁	L	17	2.41
◖	M	20	1.52
▽	N	24	1.52
▽	Q	29	1.93
◿	R	33	2.08
◸	S	36	2.08

Figure 9. - Minimum accelerator grid voltage as a function of beam current for the grids of Table III ($V_I \approx 1100$ v).
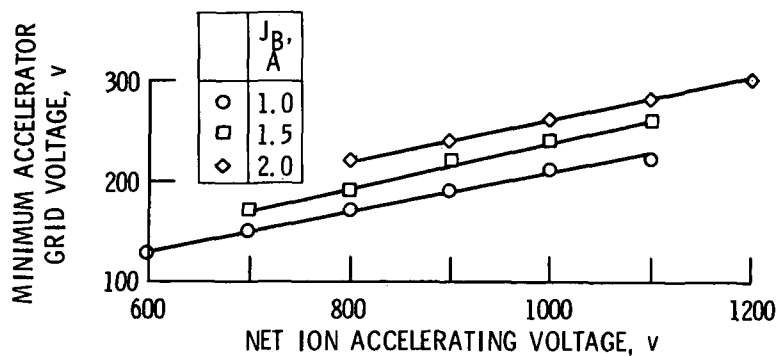

	J_B, A
○	1.0
□	1.5
◇	2.0

Figure 10. - Minimum accelerator grid voltage as a function of net ion accelerating voltage for grid set M, test 20.
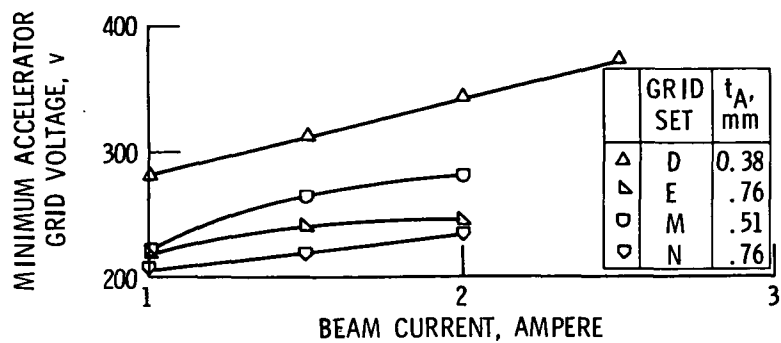
Figure 11. – Variation of the minimum accelerator grid voltage with accelerator grid thickness.
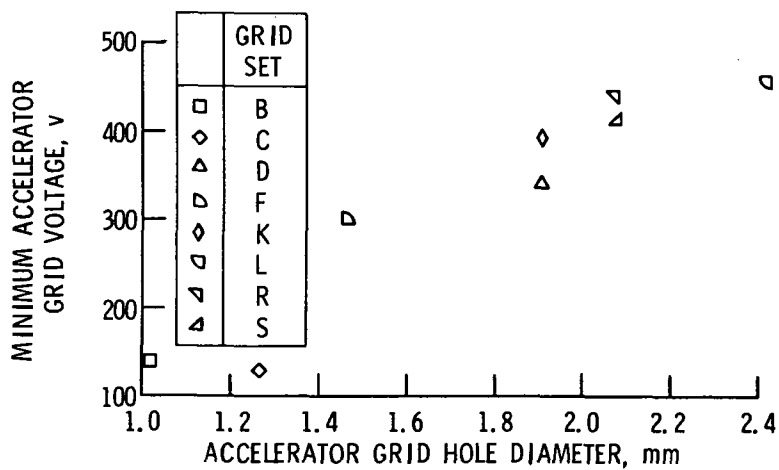

Figure 12. – Minimum accelerator grid voltage as a function of accelerator grid hole diameter for grids with accelerator grid thickness of 0.38 millimeter and beam current of 2.0 amperes.